Supplementary Information (SI) for Journal of Materials Chemistry A.
This journal is © The Royal Society of Chemistry 2026

Additive Free Co-Lean Ternary NiCoAl/Ni Foam Electrode for High-Efficiency Energy Storage and Low-Grade Heat Harvesting

P. Rupa Ranjani [a, b, c], Anjali Ashokan [b], Subhajit Biswas [b, c], Justin D. Holmes [b,c] and Kafil M. Razeeb [a*]

[a] *Micro-Nano System Centre, Tyndall National Institute, Cork T12 R5CP, Ireland.*

[b] *School of Chemistry, University College Cork, Cork T12 YN60, Ireland.*

[c] *Environmental Research Institute, University College Cork, Cork, T23 XE10, Ireland.*

Corresponding authors: kafil.mahmood@tyndall.ie

Effect of Al Content on NiCoAl LDH Composition

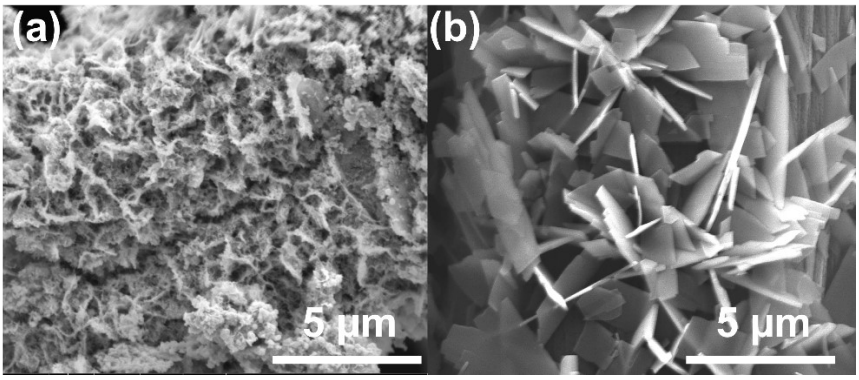

Fig. S1 SEM images of Ni-Co-Al LDH electrodes prepared at different Ni: Co:Al ratios. (a) High-Al composition $Ni_{0.33}Co_{0.17}Al_{0.50}$ (4:2:6) showing a continuous, amorphous particle network. (b) Intermediate-Al composition $Ni_{0.44}Co_{0.22}Al_{0.33}$ (4:2:3) showing irregular, plate-like LDH structures with random orientation and non-uniform thickness.

1. Experimental

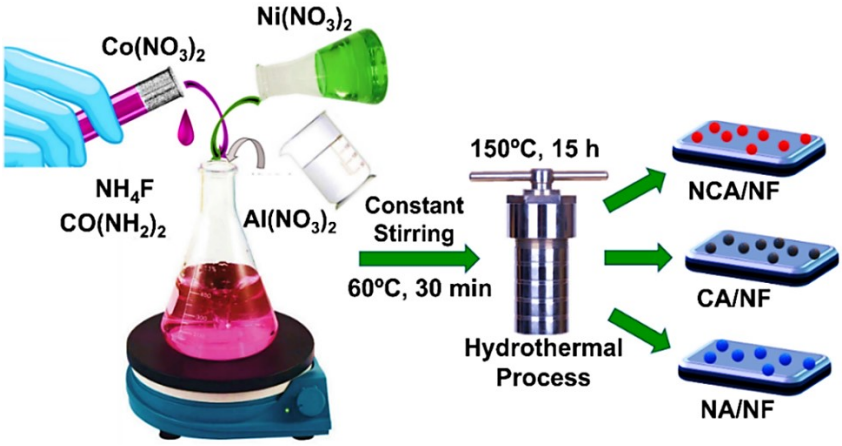

Scheme S1. Hydrothermal synthesis of LDH/NF materials.

1.1. Electrochemical measurements

The specific capacity (mAh g^{-1}) was calculated from the discharge curves in accordance with the following equation,

$$C_s = \frac{I \times t}{3.6 \times m} \qquad (S1)$$

Similarly, the specific capacitance (F g^{-1}) in the three-electrode system can be determined using equation,

$$C_s = \frac{I \times \Delta t}{m \times \Delta V} \qquad (S2)$$

where, I is the current (mA), Δt is the discharge time (s), m is the mass loading of active material (mg), and ΔV is the cell voltage.

The standard formula to calculate areal capacitance C_A from galvanostatic charge/discharge (GCD) data is:

$$C_A = \frac{I\,\Delta t}{A\,\Delta V} \qquad (S3)$$

Where C_A is the areal capacitance (F cm^{-2}), I is the discharge current (A), Δt the discharge time (s), A is s the geometric area of the electrode (cm^2), and ΔV is the potential window during discharge (V), excluding IR drop.

The capacitance of asymmetric supercapacitor device can be calculated using the equation,

$$C_s = \frac{I_{cell} \cdot \Delta t}{m_{total} \cdot \Delta V} \quad (S4)$$

Where C_s is the specific capacitance, where I_{cell} is the discharge current, Δt is the discharge time, $m_{total}$is the total mass of active material, and ΔV is the discharge voltage window.

The formula for calculating the mass loading of the negative electrode (m$^-$) is provided in the subsequent section.

$$\frac{m^+}{m^-} = \frac{C_- \times \Delta E_-}{C_+ \times \Delta E_+}$$

where, m^+ denotes the mass loading of the positive electrode; C_- and C_+ represent the specific capacities of the negative and positive electrodes, respectively, while ΔE_- and ΔE_+ indicating the corresponding potential limits. The specific energy (S_E) and specific power (S_P) of the ASC can be calculated using the following equations [1,2]:

$$S_E = \frac{C_s \times V^2}{2 \times 3.6} \; Wh\, kg^{-1} \quad (S6)$$

$$S_P = \frac{S_E \times 3600}{\Delta t} \; W\, kg^{-1} \quad (S7)$$

where C_s, V and Δt, are the Capacitance, the operating potential window, and the discharge time of ASC.

1.2. Thermo-electrochemical measurements

$$S_e = \frac{\Delta V}{\Delta T} \quad (S8)$$

where, ΔV is the change in open circuit voltage and ΔT is the temperature gradient.
The heat energy Q_{dis} associated with the chemical reaction in the TEC can be determined using the following equation [3]:

$$Q_{dis} = T_H \Delta S \quad (S9)$$

Here, T_H refers to the operating temperature of the TEC, and ΔS represents the entropy change, which is equal to the sum of the entropy changes at both the positive and negative electrodes.

Reproducibility Note: All supercapacitor measurements (CV, GCD, rate capability, cycling stability, Nyquist analysis) were repeated thrice (n = 3) on independently fabricated NCA/NF electrodes. Isothermal characteizations and TEC measurements (OCV-ΔT) were repeated also triplicated (n = 3). All datasets showed consistent trends with no anomalous variations.

2. Growth Mechanism of 3D NiCoAl microflower

The formation of 3D LDH microflower structures on NF substrate is a result of a carefully modulated hydrothermal synthesis involving urea and ammonium fluoride (NH_4F). The growth mechanism is proposed to follow a combination of homogeneous precipitation, Ostwald ripening, and self-assembly, as supported by previous reports. Initially, in the hydrothermal environment, urea undergoes hydrolysis, gradually releasing hydroxide ions (OH^-) and carbonate species (CO_3^{2-}) according to the reaction (S10) [4,5],

$$CO(NH_2)_2 + H_2O \rightarrow 2NH_3 + CO_2 \quad (S10)$$

$$CO_2 + H_2O \rightarrow CO^{2-}_3 + 2H^+$$

$$NH_3 + H_2O \rightarrow NH^+_4 + OH^-$$

The generation of OH^- facilitates the co-precipitation of metal hydroxides from the mixed metal precursor solution containing Ni^{2+}, Co^{2+}, and Al^{3+} ions. Concurrently, complexation occurs between the metal cations and ammonia ligands as given in reaction (S11),

$$Ni^{2+} + 4NH_3 \rightleftharpoons [Ni(NH_3)_4]^{2+} \quad (S11)$$

$$Co^{2+} + 4NH_3 \rightleftharpoons [Co(NH_3)_4]^{2+}$$

$$Al^{3+} + 6NH_3 \rightleftharpoons [Al(NH_3)_6]^{3+}$$

These complexes release metal ions in a controlled manner under hydrothermal conditions. The slowly released Ni^{2+}, Co^{2+}, and Al^{3+} ions react with OH^- to form their respective hydroxide phases as given in the reaction (S12),

$$[Ni(NH_3)_4]^{2+} + 2OH^- \rightarrow Ni(OH)_2 + 4NH_3 \quad (S12)$$

$$[Co(NH_3)_4]^{2+} + 2OH^- \rightarrow Co(OH)_2 + 4NH_3$$

$$[Al(NH_3)_6]^{3+} + 3OH^- \rightarrow Al(OH)_3 + 6NH_3$$

The addition of NH_4F during synthesis plays a pivotal role in directing the growth of 3D NiCoAl-LDH microstructures. Fluoride ions (F^-) form complexes with metal cations, enabling controlled release of Ni^{2+}, Co^{2+}, and Al^{3+} into the reaction medium, thereby regulating nucleation and promoting anisotropic crystal growth. Concurrently, ammonium ions (NH_4^+) help maintain a stable pH environment conducive to layered double hydroxide formation. The F^- ions further facilitate the oriented stacking of hexagonal LDH nanosheets through multidirectional growth and enhanced surface energy anisotropy, leading to the development of well-defined 3D hierarchical architectures as shown in Fig. 1(b). In parallel, $Al(OH)_3$ may form as amorphous or spherical intermediates that act as nucleation templates for the assembly of LDH nanosheets. Subsequently, through a self-assembly process governed by Ostwald ripening, the LDH nanosheets evolve into highly porous, flower like superstructures [5]. These micro-flowers, typically ranging from 2 to 5 μm in diameter, exhibit uniform distribution on the NF substrate.

3. Results and discussions

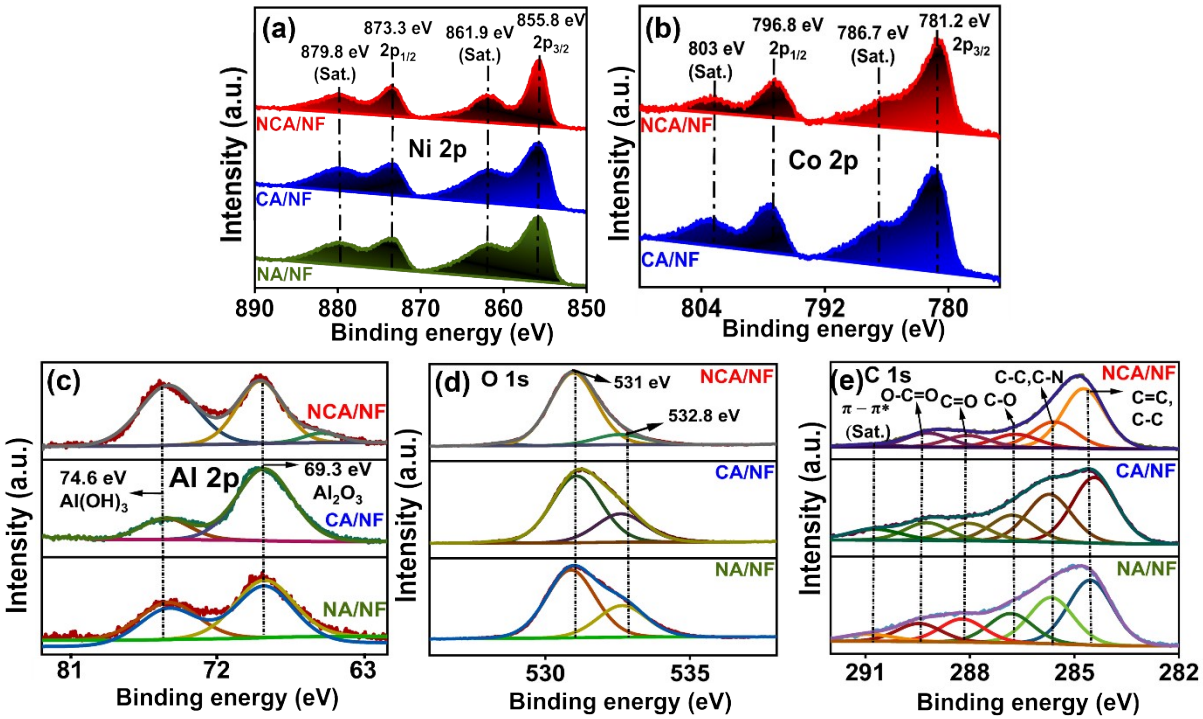

Fig. S2 High resolution XPS spectra of LDH/NF (a) Ni 2p, (b) Co 2p, (c) Al 2p, (d) O 1s, & (e) C 1s.

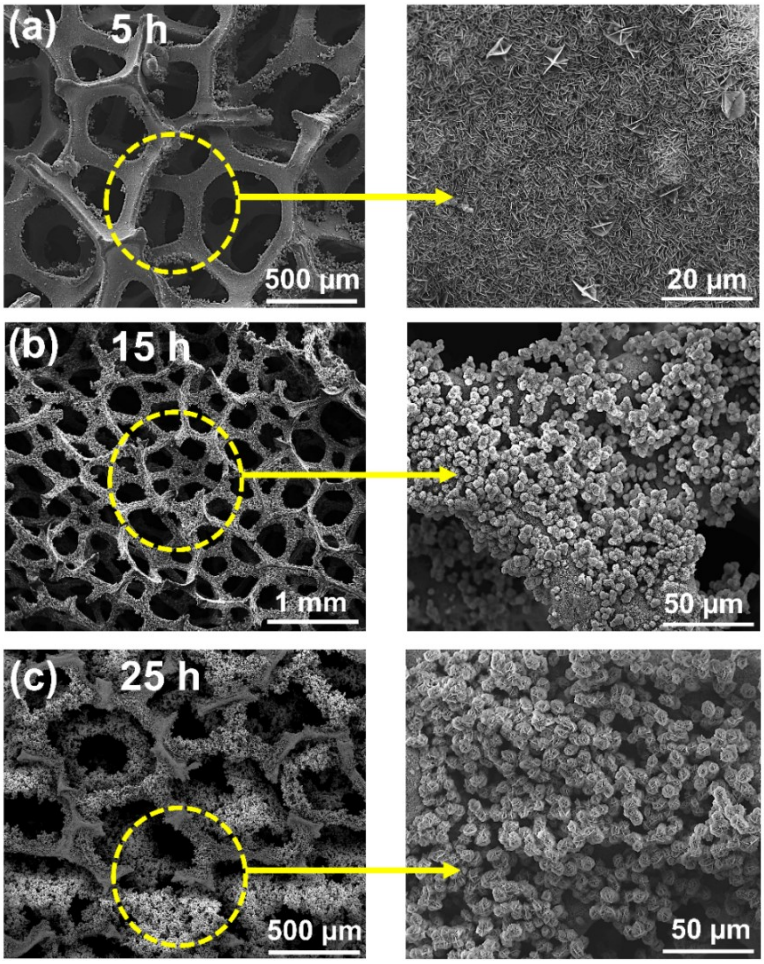

Fig. S3 FE-SEM images of hydrothermally synthesised NCA/NF at (a) 5 h, (b) 15 h and (c) 25 h.

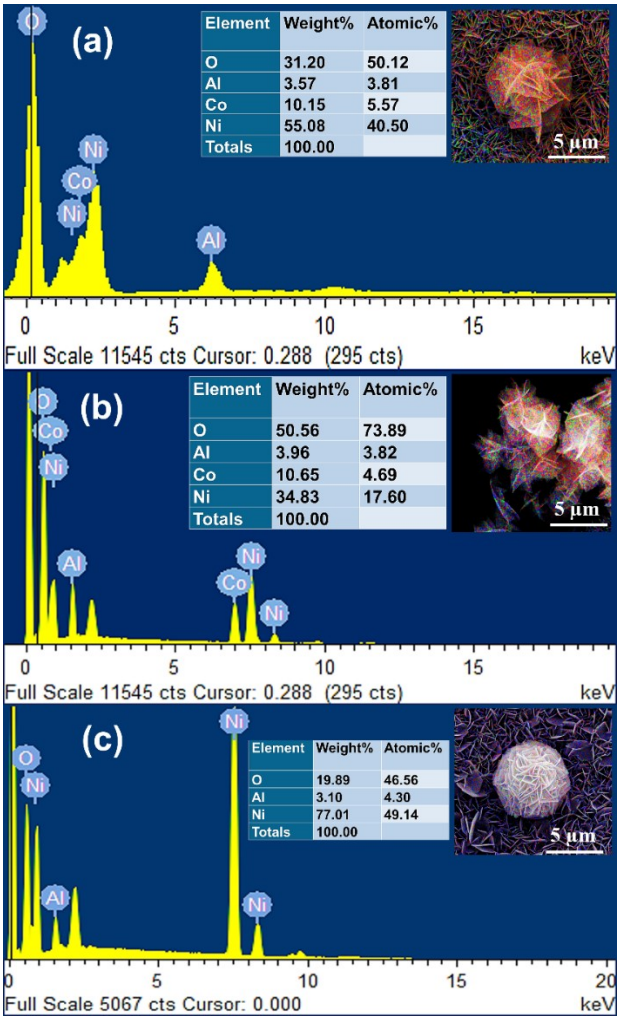

Fig. S4 EDX spectra and elemental mapping a) NCA/NF, b) CA/NF and c) NA/NF electrodes.

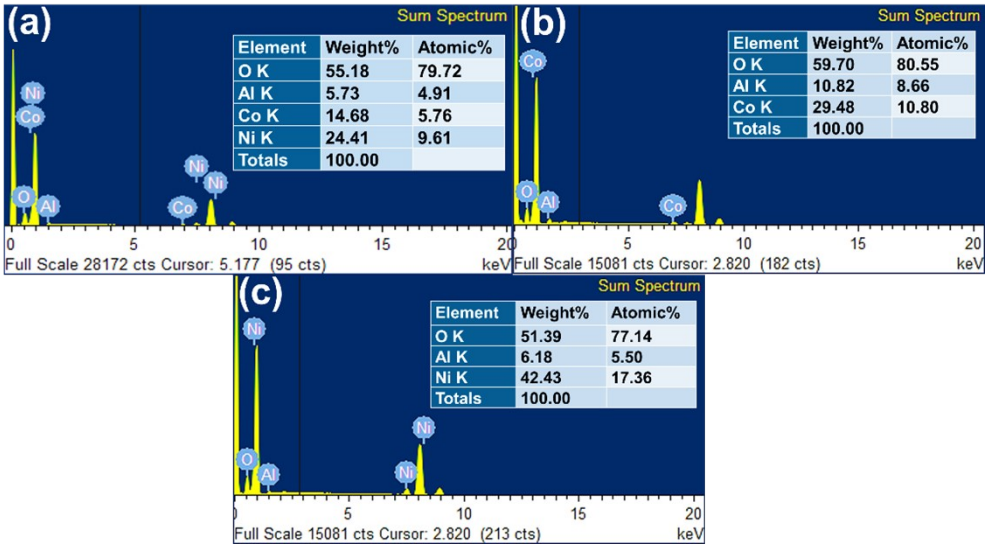

Fig. S5 EDX spectra a) NiCoAl-LDH, b) CoAl-LDH and c) NiAl-LDH powder samples.

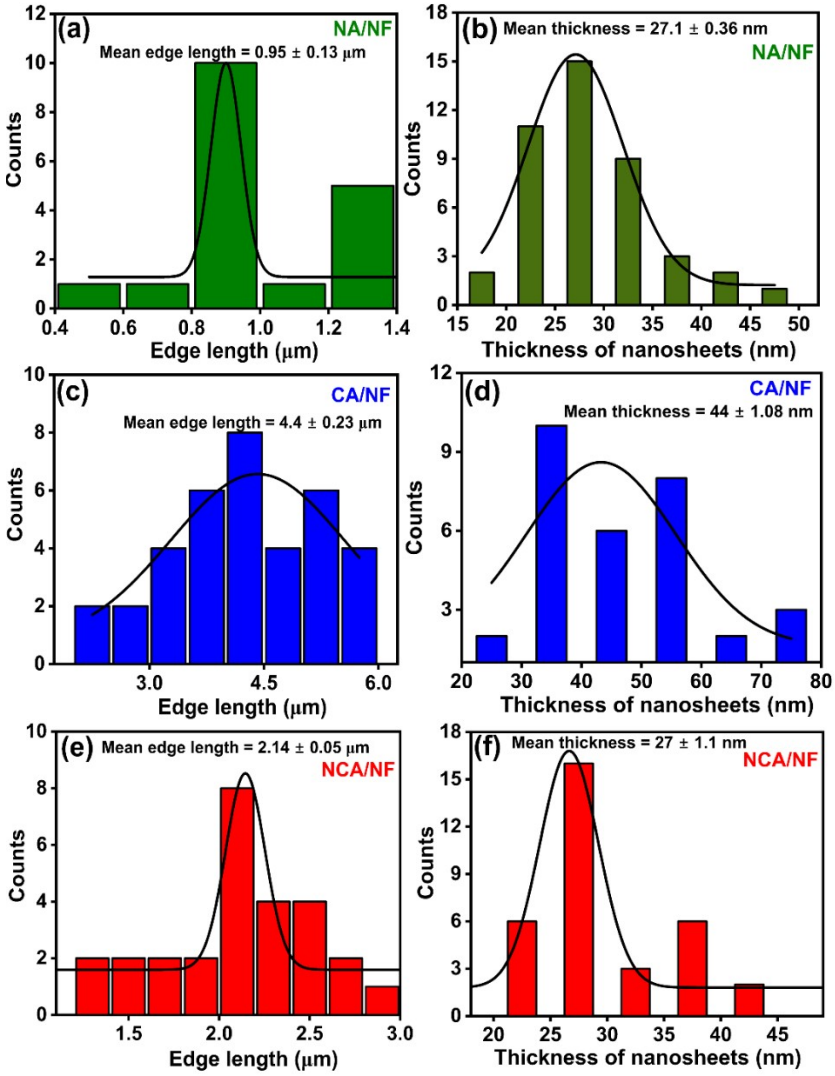

Fig. S6 Histogram analysis of the edge length and nanosheet thickness distributions for (a-b) NA/NF, (c-d) CA/NF, and (e-f) NCA/NF microflowers obtained from SEM images.

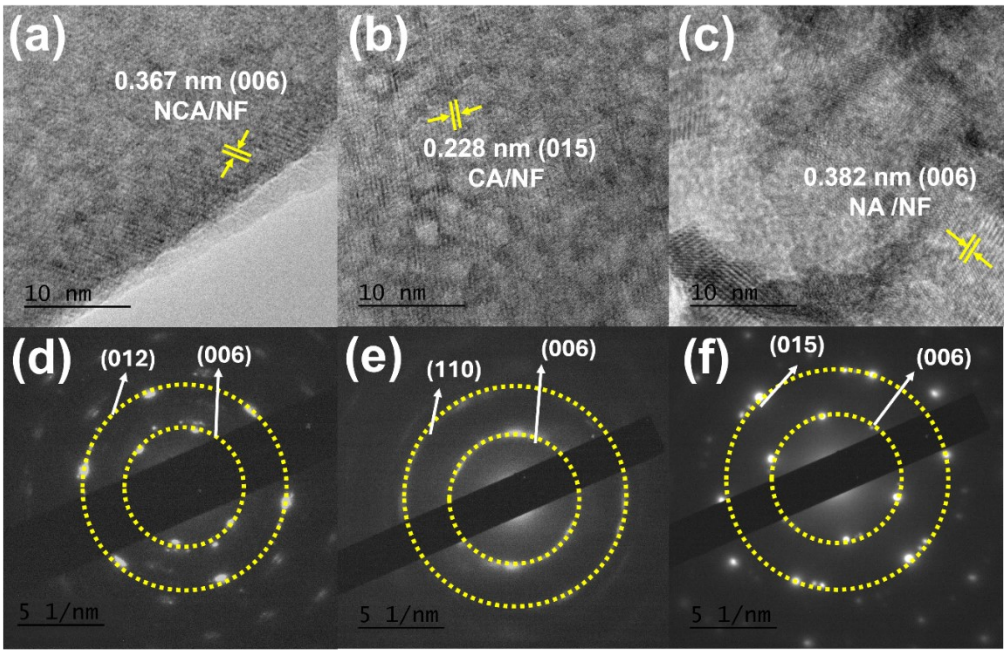

Fig. S7 (a-c) HRTEM images and (d-f) SAED pattern of LDH/NF electrodes.

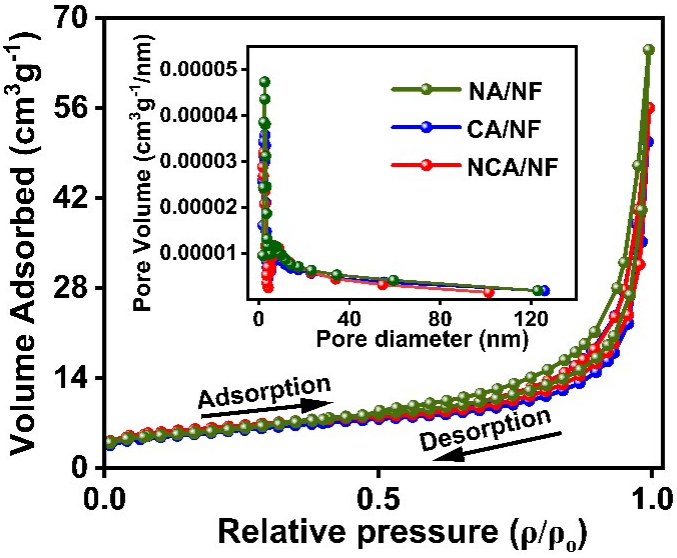

Fig. S8 Nitrogen adsorption-desorption isotherms to determine the surface area with the inset graph representing pore size distributions of NA/NF, CA/NF and NCA/NF electrodes.

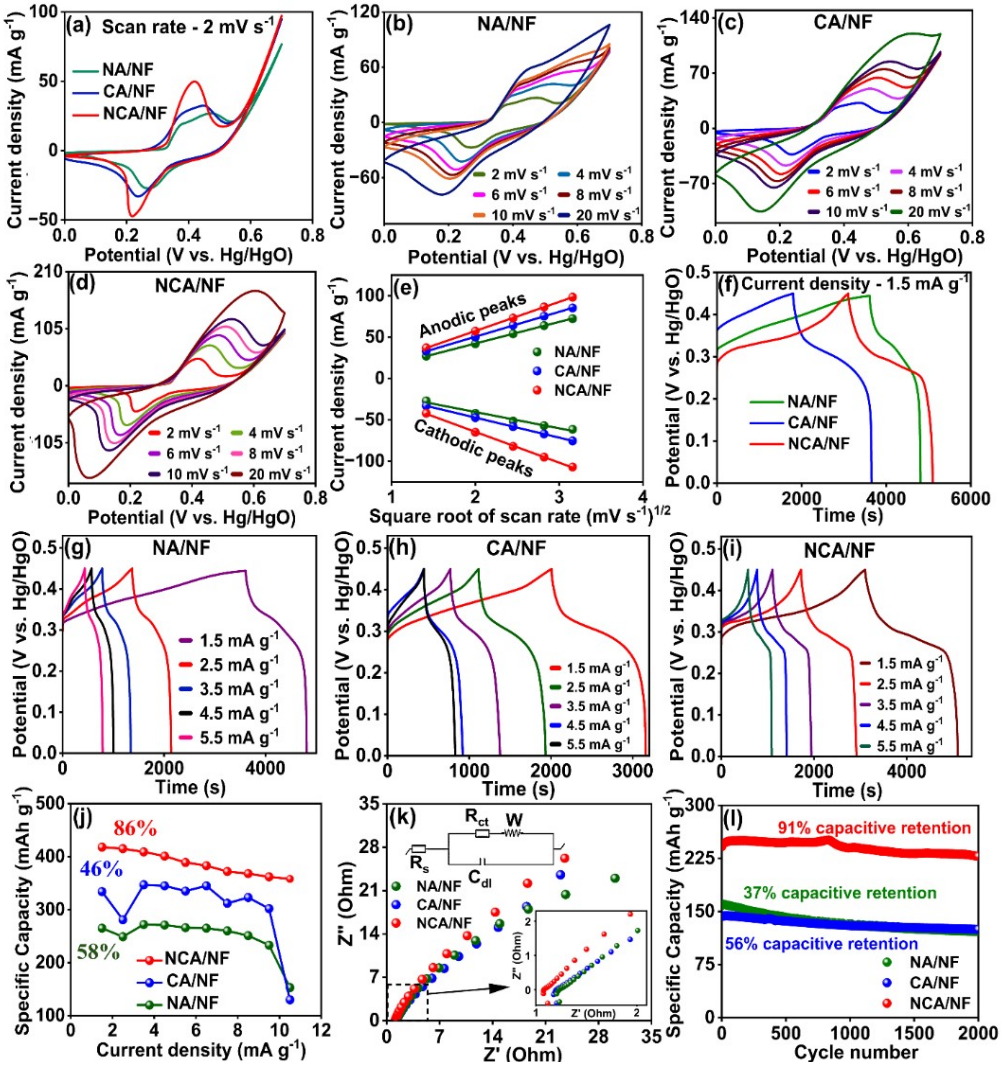

Fig. S9 (a) Comparative CV plots at a scan rate of 2 mVs^{-1} , (b-d) CV curves at various scan rates from 2 to 20 mV s^{-1}, (e) Relationship between anodic and cathodic peak currents as a function of square root of scan rate (In all cases, the R^2 linear fit is close to 0.99), (f) Comparative GCD curves at a current density of 1.5 mA g^{-1}, (g-i) GCD profile at various current densities from 1.5 to 5.5 mA g^{-1}, (j) Comparing the specific capacities at various current densities, (k) Nyquist plots (inset graph represents the Nyquist plot in the high frequency region), and (l) Stability curve (2000 cycles) of NA/NF, CA/NF and NCA/NF electrodes.

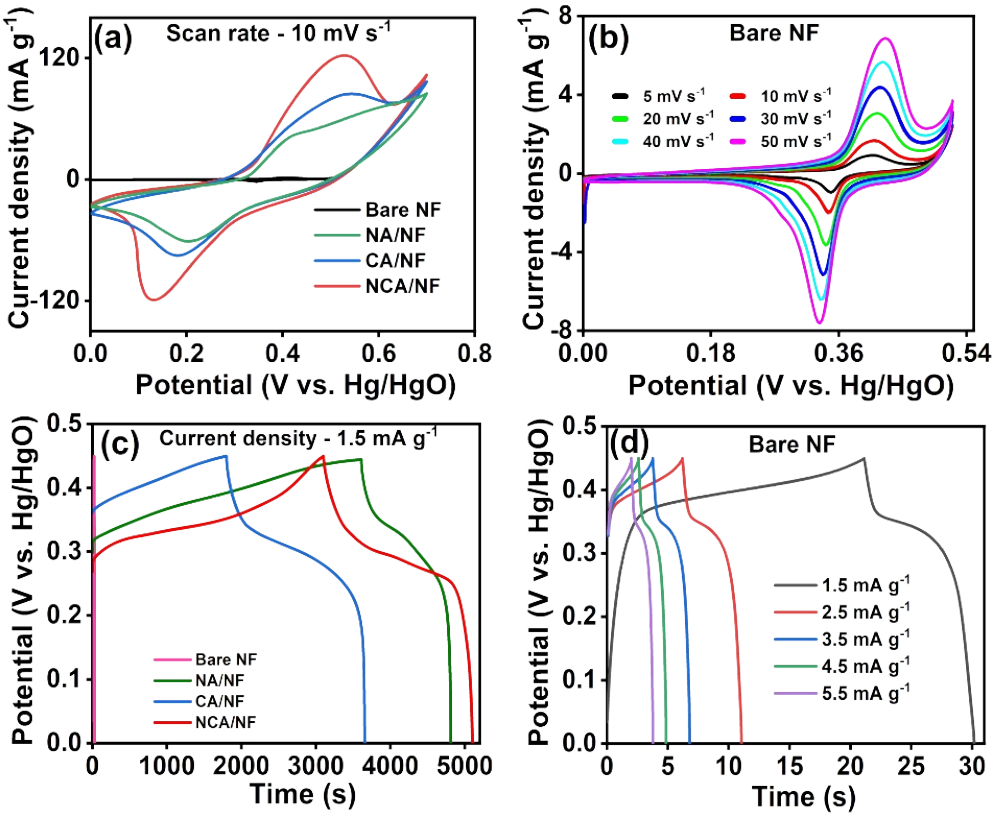

Fig. S10 Electrochemical comparison of bare Ni foam (NF) and LDH/NF electrodes. (a) CV curves of bare NF, NA/NF, CA/NF and NCA/NF at 10 mV s^{-1} , (b) CV profiles of bare NF recorded from 5-50 mV s^{-1}, (c) GCD curves of bare NF, NA/NF, CA/NF and NCA/NF at 1.5 mA g^{-1} and (d) GCD profiles of bare NF at current densities from 1.5 to 5.5 mA g^{-1}.

To elucidate charge storage mechanisms, CV data were analysed using the power law equation[6],

$$i = av^b \qquad (S13)$$

where, *a* and *b* are constants, *i* is the current (mA) and *v* is the scan rate (mV s^{-1}).

A b value of 1 indicates capacitive behaviour, while 0.5 denotes diffusion-limited processes. When the '*b*' value lies between 0.5 and 1 ($0.5 < b < 1$), it reflects pseudocapacitive or battery/capacitive behaviour involving a combination of surface-controlled and diffusion-controlled processes [7]. NA/NF exhibited a b value of 0.40, consistent with battery-type behaviour, whereas CA/NF (0.59) and NCA/NF (0.55) showed pseudocapacitive characteristics (Fig. S11).

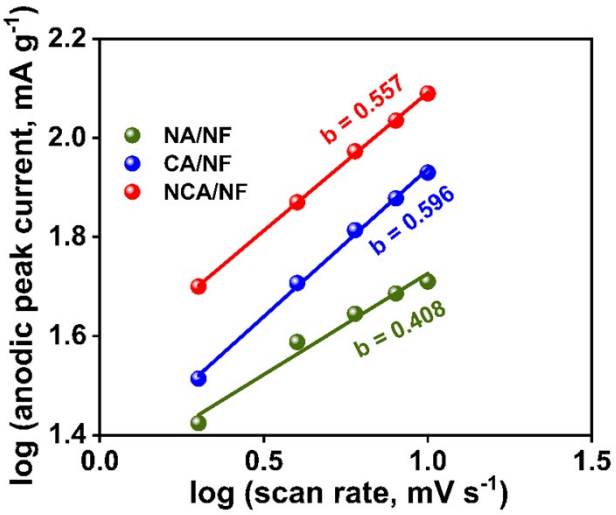

Fig. S11 Correlation between log (i) vs. log(v) at the anodic peak current density extracted from the CV curve.

The capacitive and diffusion-controlled contributions were further quantified based on the relationship between current and scan rate, expressed as the following equation,

$$i(V) = k_1 v + k_2 v^{\frac{1}{2}} \qquad (S14)$$

where v is the ramping scan rate (in mV s^{-1}), and k_1 and k_2 represent the contributions from capacitive and diffusion-controlled effects, respectively [8].

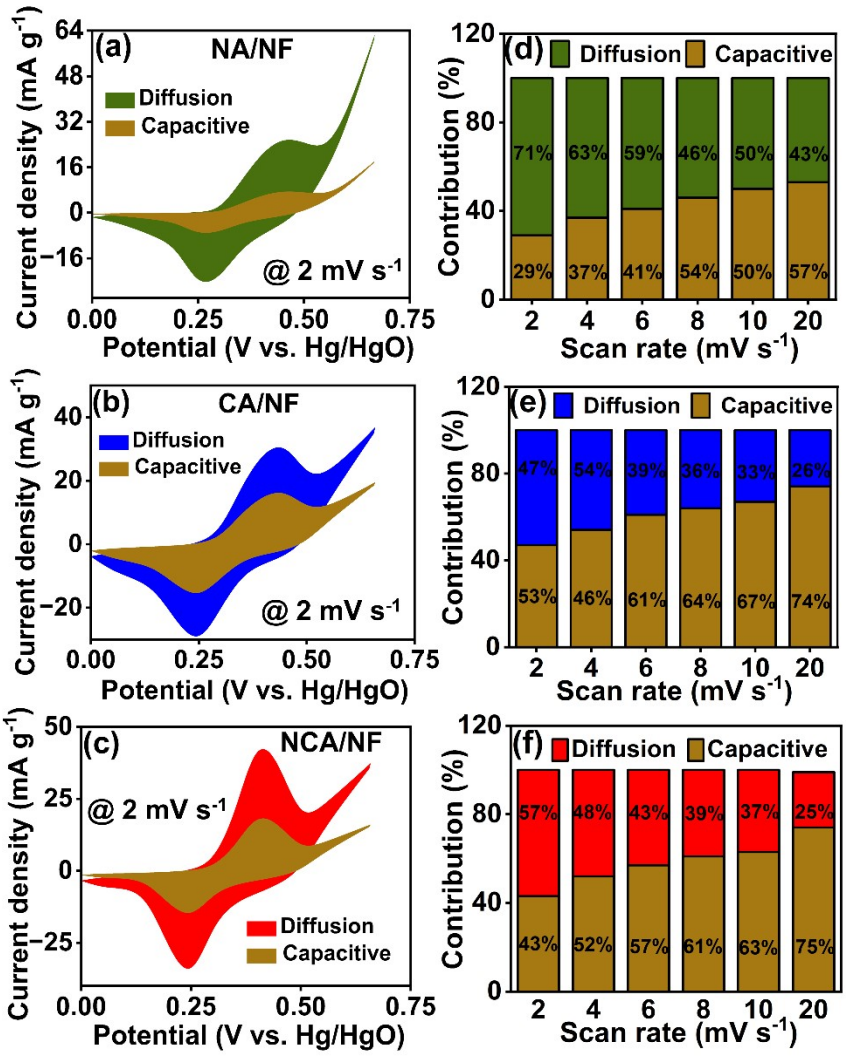

Fig. S12 (a-c) Capacitive and diffusion contributions obtained from CV scan at a scan rate of 2 mV s^{-1} (d-f) Comparison of capacitance and diffusion-controlled process at various scan rates (2 – 20 mV s^{-1}) of NA/NF, CA/NF and NCA/NF electrodes.

Table S1. Electrochemical parameters **(three electrode configuration)** of NCA/NF electrode compared with recent reports.

Electrode	Preparation method	Ni:Co:Al	Electrolyte (KOH)	Specific capacity (mAh g^{-1})	Current Density Ag^{-1}	R_{ct} (Ω)	Ref
$NiCo_2Al_{0.5}$ nanosheets	Hydrothermal (120ºC, 5 h)	1:2:0.5	3 M	210	0.5	0.25	[9]
NiCoAl-LDH nanosheets	Hydrothermal (120ºC, 10 h)	2.2:1:1.1	1 M	343.67	1	0.32	[10]
$NiCoAl_{0.1}$ LDH Nanosheet	Hydrothermal (120ºC, 5 h)	6:4:1	2 M	284.45	1	0.50	[11]
$Ni_1Co_2Al_1$-LDH	Hydrothermal (120ºC, 24 h)	1:2:1	6 M	101	1	-	[12]
NiCoAl - LDH nanosheets	Hydrothermal (150ºC, 18 h)	1:3:3	3 M	176	1	9.05	[13]
NiCoAl-LDH	Hydrothermal (120ºC, 4 h)	2:1:0.1	2 M	233	1	1.34	[14]
NCA/NF	**Hydrothermal (150ºC, 15 h)**	**4:2:1**	**1 M**	**418**	**1.5**	**0.025**	**This work**

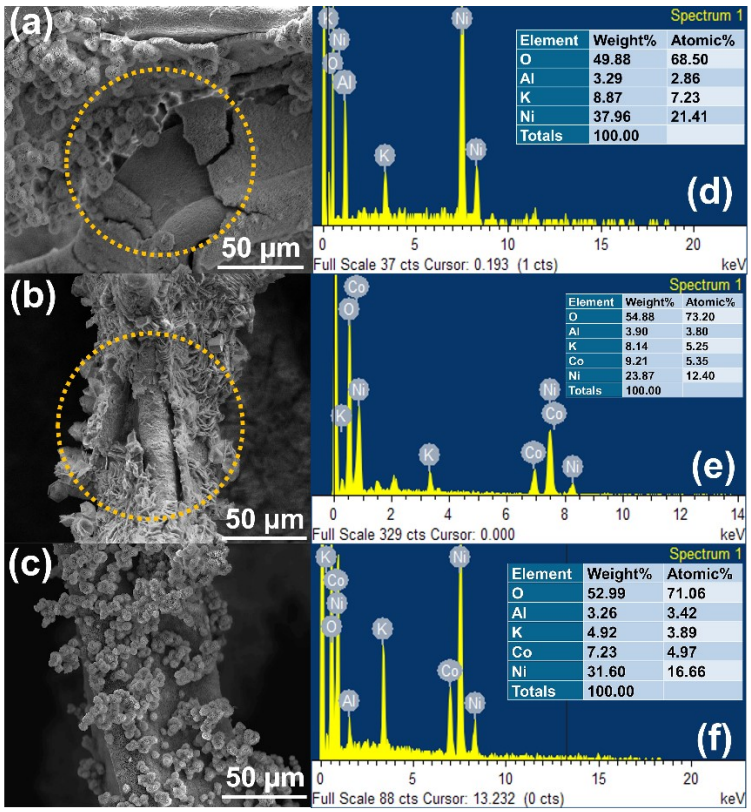

Fig. S13 Post-cycling studies after 2000 cycles: (a-c) SEM images and (d-f) EDX spectra of LDH/NF electrodes.

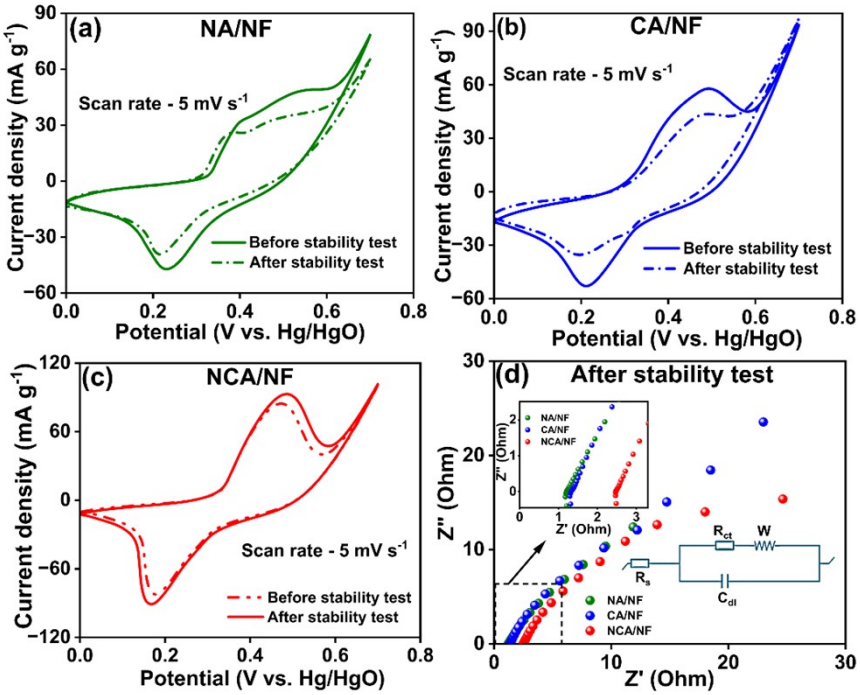

Fig. S14 Post-cycling studies after 2000 cycles (a-c) CV profile and (d) Nyquist plots, before and after cyclic stability test of NA/NF, CA/NF and NCA/NF electrodes.

Table S2. Parameters calculated from Nyquist Plot

Electrodes	**Before Cyclic Stability**		**After Cyclic Stability**	
	$R_s\,(\Omega)$	$R_{ct}\,(\Omega)$	$R_s\,(\Omega)$	$R_{ct}\,(\Omega)$
NA/NF	1.21	0.031	1.21	0.034
CA/NF	1.24	0.036	1.31	0.09
NCA/NF	1.18	0.025	2.49	0.038

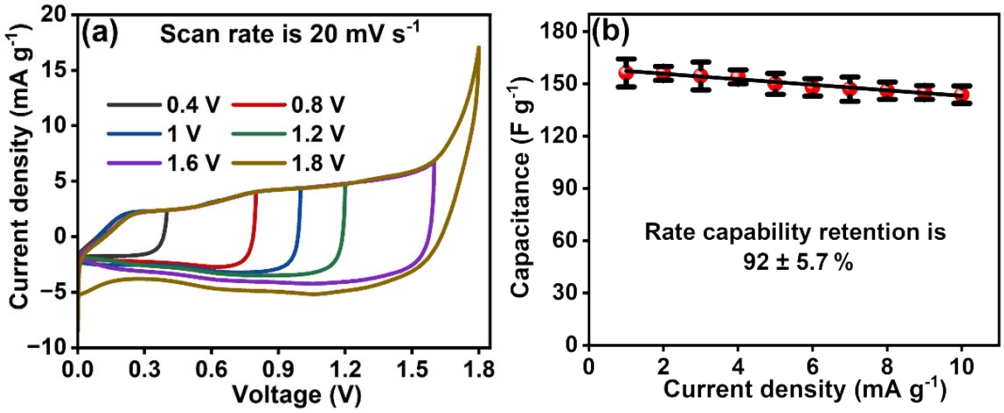

Fig. S15 (a) Optimising potential window of NCA/NF//AC/NF ASC from 0.4 – 1.8V, (b) Rate capability of NCA/NF//AC/NF ASC device at different current densities. Measurements were triplicated (n = 3). Data are presented as mean ± standard deviation (SD), with error bars representing electrode-to-electrode variability (e.g., 92% ± 5.7%). All datasets showed consistent trends across replicates.

3.1. Device-Level Performance Calculations for NCA/NF//AC/NF ASC

In this work, we report all device-level electrochemical performance values (specific capacitance in F g^{-1}, and specific energy in Wh kg^{-1}) on a total active mass basis. This means that the mass of the positive and negative electrodes together is used in all calculations. We do not use a single-electrode mass basis for device-level data.
The mass loadings used in our assembled device were:

- Positive electrode (NCA/NF): 1.5 mg cm^{-2}
- Negative electrode (AC/NF): 2.5 mg cm^{-2}
- Electrode area: 1 cm^2

The total active mass of NCA/NF//AC/NF ASC device is:

$$m_{\text{total}} = m_{+} + m_{-} = 0.0015\ \text{g} + 0.0025\ \text{g} = 0.0040\ \text{g}$$

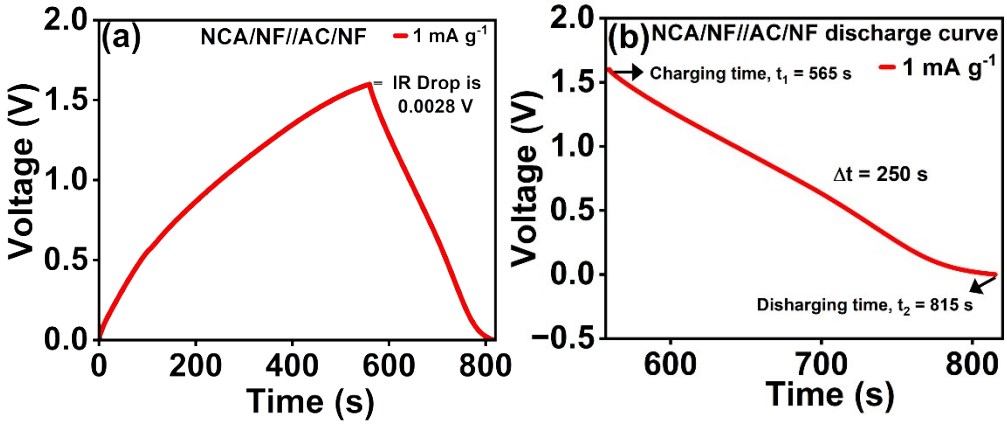

Fig. S16 (a) Galvanostatic charge–discharge (GCD) profile of the NCA/NF//AC/NF asymmetric supercapacitor (ASC) at 1 mA g^{-1}, exhibiting a negligible IR drop of 0.0028 V. (b) Corresponding discharge curve at 1 mA g^{-1}, highlighting the well-defined charge and discharge intervals.

The device was operated over a 0-1.6 V window. However, the true electrochemical window must be corrected for the internal resistance (R_s) of the device. This avoids overestimating performance due to an instantaneous voltage drop at the beginning of discharge[15].
The ohmic resistance from EIS was:

$$R_s = 0.70\ \Omega$$

At a current density of 1 A g^{-1}, the actual current in the cell is:
$I_{\text{cell}} = 1\ \text{mA/mg} \times 4\ \text{mg} = 0.0040\ \text{A}$

Therefore, the IR drop is:
$\text{IR drop} = I_{\text{cell}} \times R_s = 0.0040\ \text{A} \times 0.70\Omega\ = 0.0028\ \text{V}$

These equations directly connect raw discharge behaviour to the reported performance values.

This is only 2.8 mV, which is negligible compared to 1.6 V. After correction, the operational voltage window remains:

$V_{\text{corrected}} = 1.6$ V

By explicitly accounting for the IR-drop, we ensure that all performance metrics are extracted from real usable voltage, not an inflated value. The following standard electrochemical relations were used,[16,17]

Device capacitance:

$$C_{\text{cell}} = \frac{I_{\text{cell}}\,\Delta t}{m_{\text{total}}\,\Delta V}$$

To determine the correct value of I_{cell}, it is important to express the applied current in absolute units (A or mA) and not in normalised unit (mA g^{-1} or A g^{-1}).

Given:

- Current density: $J = 1\text{mA}\ g^{-1}$
- Total mass: $m_{\text{total}} = 4\text{ mg} = 0.004\text{ g}$
- Δt = 250 s
- Voltage window: ΔV = 1.6 V

Step 1: Convert current density to absolute current

Current density is the applied current normalised to the total active mass:

$$J = \frac{I_{\text{cell}}}{m_{\text{total}}}$$

Rearranging:

$I_{\text{cell}} = J \times m_{\text{total}}$

$I_{\text{cell}} = J \times m_{\text{total}} = 1\text{ mA/mg} \times 4\text{ mg} = 4\text{ mA} = 4 \times 10^{-3}\text{ A}$

Step 2: Capacitance calculation

$$C_{\text{cell}} = \frac{I_{\text{cell}} \cdot \Delta t}{m_{\text{total}} \cdot \Delta V}$$

Substitute values:

$$C_{\text{cell}} = \frac{4 \times 10^{-3}\text{ A} \times 250\text{ s}}{0.004\text{ g} \times 1.6\text{ V}}$$

Numerator:

$4 \times 10^{-3} \times 250 = 1.0\ Coulomb$

Denominator:

$0.004g \times 1.6V = 0.0064\ g.V$

$$C_{\text{cell}} = \frac{1.0\ Coulomb\ (Q)}{0.0064\ g.V} \qquad = 156.25\ \text{F g}^{-1}$$

Note:

$$\frac{\text{Q}}{\text{V}} = Farad\ (F)$$

$$\frac{\text{Q}}{\text{V}.g} = \text{F g}^{-1}$$

Specific Energy (S_E, in Wh kg^{-1})

Given:

- Device capacitance = 156.25 F g^{-1}
- Corrected operating voltage = 1.6 V

Formula

$$S_E = \frac{0.5\ C_s\ V^2}{3.6}$$

Substitute values

$$S_E = \frac{0.5 \times 156.25 \times (1.6)^2}{3.6}$$

Calculate

$$(1.6)^2 = 2.56$$

$$0.5 \times 156.25 = 78.125$$

$$78.125 \times 2.56 = 199.6$$

Final energy

$$S_E = \frac{199.6}{3.6} = 55.4\ \text{Wh kg}^{-1}$$

Specific Power

(W kg^{-1})

$$S_P = \frac{S_E \times 3600}{\Delta t}\ W\ kg^{-1}$$

Given:

- $S_E = 55.4\ \text{Wh kg}^{-1}$
- $\Delta t = 250$ s

Step 1: Convert Wh to W·s:

$$S_E \times 3600 = 55.4\ Wh\ kg^{-1} \times 3600 = 1994400\ W.s\ kg^{-1}$$

Step 2: Divide by discharge time:

$$S_P = \frac{199440\ W.s\ kg^{-1}}{250\ s}$$

Final Specific power

$$S_P = 797.76\ \text{W kg}^{-1}$$

The capacitance, specific energy, and specific power values reported at all other current densities were calculated using the same procedure described above.

The positive and negative electrodes were deliberately not assigned equal masses. Instead, their masses were selected to ensure charge balance, which is essential in asymmetric devices. The balancing follows:

$$\frac{m^+}{m^-} = \frac{C_- \Delta E_-}{C_+ \Delta E_+}$$

Using the *device-relevant* capacitance values (at 20 mA g^{-1}):

- $C_+ = 900\ \text{F g}^{-1}$, $\Delta E_+ = 0.5\ \text{V}$
- $C_- = 210\ \text{F g}^{-1}$, $\Delta E_- = 1.2\ \text{V}$

$$\frac{m^+}{m^-} = \frac{210 \times 1.2}{900 \times 0.5} = \frac{252}{450} = 0.56$$

The experimentally used ratio is:

$$\frac{1.5\ \text{mg}}{2.5\ \text{mg}} = 0.60$$

The excellent galvanostatic discharge symmetry, voltage retention, and cycling stability confirm that the cell is correctly mass balanced.

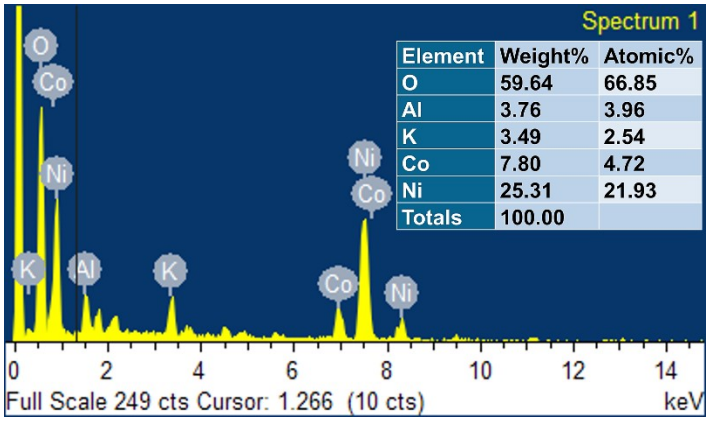

Fig. S17 Post electrochemical study: EDX spectra of NCA/NF electrode after 25,000 cycles.

3.2. Isothermal characterization

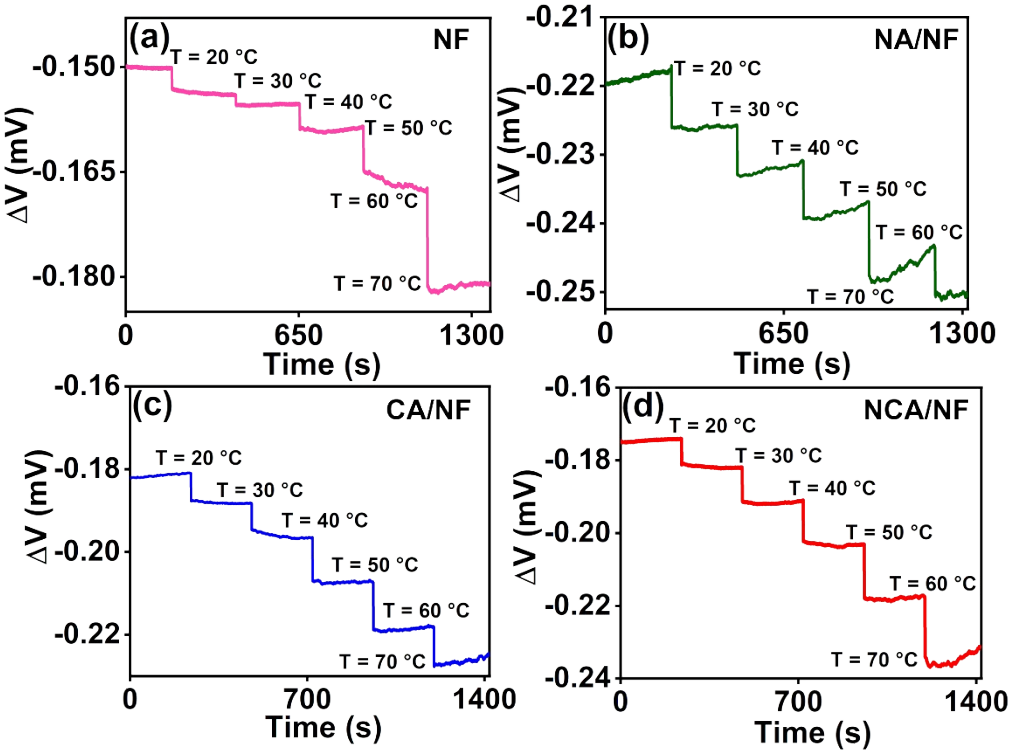

Fig. S18 Stepwise isothermal (uniform-temperature rise) OCV measurement of (a) Bare NF, (b)NA/NF, (c) CA/NF and NCA/NF electrodes.

These contributions can be quantitatively partitioned using the following relationships as proposed in the previous reports [18,19],

$$Thermodiffusion\ \% = \frac{|TC(diffusion)|}{|TC\ (total)|} \qquad (S15)$$

$$Thermogalvanic\ \% = \frac{|TC(Redox)|}{|TC\ (total)|} \qquad (S16)$$

$$TC(redox) = TC(total) - TC(diffusion)$$

3.3. Non-isothermal characterization

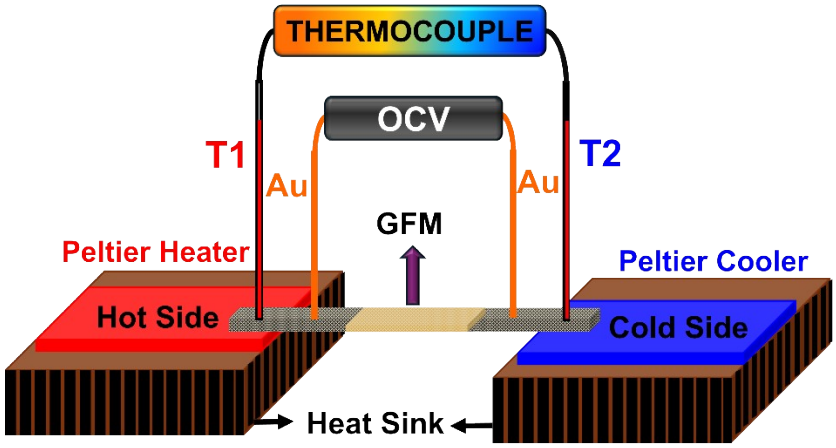

Fig. S19 Scheme of non-isothermal Seebeck coefficient measurement setup.

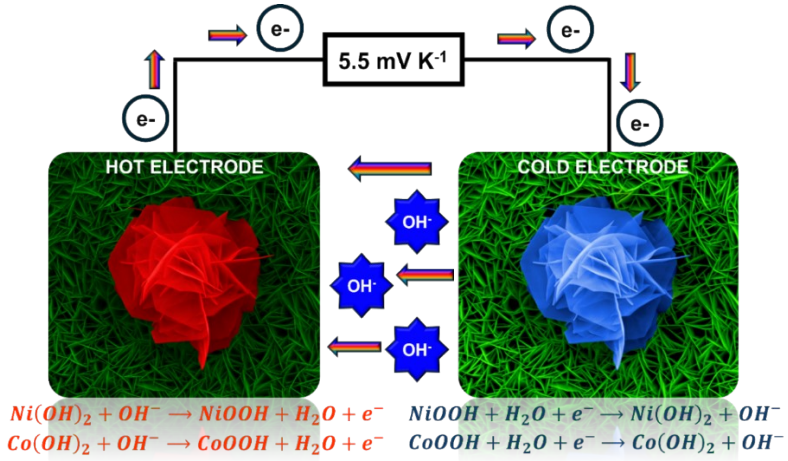

Fig. S20 Schematic of NCA/NF | GFM | NCA/NF TEC mechanism.

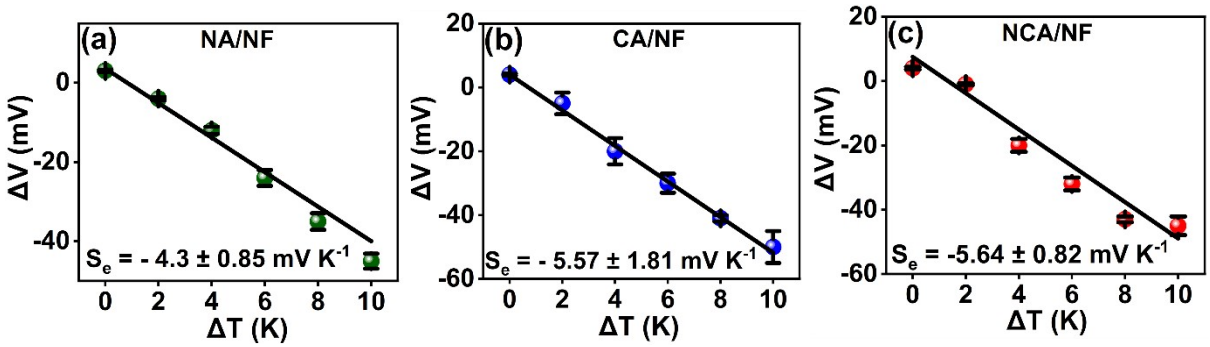

Fig. S21 Polarity-flip test for symmetric (a) NA/NF, (b)CA/NF and (c) NCA/NF LDH electrodes in a transverse thermoelectrochemical cell.

References

1 P. Rupa Ranjani, P. M. Anjana and R. B. Rakhi, *J Energy Storage*, DOI:10.1016/j.est.2020.102063.

2 X. Li, W. Yan, S. Guo, Y. Liu, J. Niu, L. Yin and Z. Wang, *Electrochim Acta*, DOI:10.1016/j.electacta.2021.138488.

3 J. Duan, B. Yu, L. Huang, B. Hu, M. Xu, G. Feng and J. Zhou, *Cell Press*, 2021, preprint, DOI: 10.1016/j.joule.2021.02.009.

4 W. Y. Lim and G. W. Ho, *Procedia Eng*, 2017, **215**, 163–170.

5 E. Boccalon, G. Gorrasi and M. Nocchetti, *Elsevier B.V.*, 2020, preprint, DOI: 10.1016/j.cis.2020.102284.

6 G. P. Ojha, B. Pant, J. Acharya, P. C. Lohani and M. Park, *Chemical Engineering Journal*, DOI:10.1016/j.cej.2023.142621.

7 M. Bhatt, B. Gupta and A. K. Sinha, *Sci Rep*, DOI:10.1038/s41598-025-85113-z.

8 R. M. Ghanem, D. A. Kospa, A. I. Ahmed, A. A. Ibrahim and A. Gebreil, *RSC Adv*, 2023, **13**, 29252–29269.

9 Y. Chen, Y. Ouyang, J. Yang, L. Zheng, B. Chang, C. Wu, X. Guo, G. Chen and X. Wang, *ACS Appl Energy Mater*, 2021, **4**, 9384–9392.

10 X. Wang, Y. Lin, Y. Su, B. Zhang, C. Li, H. Wang and L. Wang, *Electrochim Acta*, 2017, **225**, 263–271.

11 X. Huang, B. Chu, B. Han, Q. Wu, T. Yang, X. Xu, F. Wang and B. Li, *Small*, DOI:10.1002/smll.202401315.

12 J. Zhang, N. Sun, B. Yin, Y. Su, S. Ji, Y. Huan and T. Wei, *Dalton Transactions*, DOI:10.1039/d2dt02893j.

13 K. R. Hariprasath, M. Priyadharshini, P. Balaji, R. kumar, R. Thangappan and T. Pazhanivel, *Chem Phys Lett*, DOI:10.1016/j.cplett.2024.141584.

14 S. Zhang, Y. Zhao, S. Gao, C. Liu and X. Chen, *J Power Sources*, DOI:10.1016/j.jpowsour.2025.236370.

15 H. Peng, G. Ma, K. Sun, Z. Zhang, J. Li, X. Zhou and Z. Lei, *J Power Sources*, 2015, **297**, 351–358.

16 K. Li, X. Wang, X. Wang, M. Liang, V. Nicolosi, Y. Xu and Y. Gogotsi, *All-Pseudocapacitive Asymmetric MXene-Carbon-Conducting Polymer Supercapacitors 2*, 2020.

17 R. Isci, K. B. Donmez, Z. Cobandede, B. Chakrabarti, N. Karatepe and T. Ozturk, *J Mater Chem A Mater*, 2025, **13**, 39887–39902.

18 Z. Li, Y. Xu, L. Wu, H. Dou and X. Zhang, *J Mater Chem A Mater*, DOI:10.1039/d2ta05882k.

19 Z. Li, Y. Xu, L. Wu, J. Cui, H. Dou and X. Zhang, *Nat Commun*, DOI:10.1038/s41467-023-42492-z.